Q. J. R. Meteorol. Soc. (2000), **126**, pp. 2323–2350

Distinguishing between the SST-forced variability and internal variability in mid latitudes: Analysis of observations and GCM simulations

By DAVID M. STRAUS* and J. SHUKLA
Center for Ocean–Land–Atmosphere Studies, USA

(Received 4 March 1999; revised 4 August 1999)

SUMMARY

It is shown that the dominant structure of the seasonal-mean mid-latitude circulation (500 hPa height) pattern over the Pacific–North America (PacNA) region forced by tropical sea surface temerature (SST)-related diabatic heating, is distinctly different from the seasonal-mean internal variability pattern that occurs in the absence of El Niño Southern Oscillation (ENSO) related SST anomalies. The separation of these two patterns is accomplished by utilizing ensemble General Circulation Model (GCM) integrations in conjunction with re-analyses.

Ensemble simulations made with the GCM of the Center for Ocean–Land–Atmosphere Studies (COLA) are compared to the re-analyses of the National Centers for Environmental Prediction (NCEP) for the 16 winters 1981/82–96/97. The GCM ensemble for each winter consists of 9 integrations initialized from analyses, and utilizing the observed time-varying SST. In addition, a 39-year simulation with the same GCM using climatological SSTs (with the observed annual cycle) is used.

The hemispheric North Atlantic/Arctic pattern is the leading seasonal-mean empirical orthogonal function (EOF) for: (i) all GCM seasonal means in the ensemble simulations; (ii) the NCEP re-analyses; and (iii) the climatological SST integration. This mode is removed from these datasets.

The total seasonal-mean variance of all GCM ensemble integrations is generally quite realistic in the PacNA region. The variance of GCM seasonal-mean deviations about the ensemble mean agrees with that in the climatological SST GCM run, but is about 20% weaker than the observed variance for 29 non-ENSO winters from the NCEP re-analyses. The ratio of the SST-forced variance (obtained from the variance of ensemble means but corrected for the finite sample size) to the internal variance (from the deviations about the ensemble mean) exceeds 2.5 in the eastern Pacific and 4.5 over Mexico. It is highly significant (99% confidence level) over most of the PacNA region.

A number of techniques are used to calculate the patterns forced by SST heating and the internal variability patterns. The SST-forced mid-latitude circulation pattern is calculated in seven ways, namely: (1) as the leading EOF of the ensemble-mean GCM height field for the 16 winters; (2) as the leading mode of a singular-value decomposition (SVD) analysis of height with tropical diabatic heating from the GCM; (3) as the leading EOF (as above) for NCEP re-analyses for the same 16 winters; (4) as the leading SVD mode (as above) for the NCEP re-analyses for the same 16 winters; (5) as the leading EOF of height from re-analyses for the 10 winters having the five strongest warm and five strongest cold tropical SST anomalies in the last 39 years; (6) as the leading SVD mode (as above) from re-analyses for these same 10 extreme-SST winters; (7) as a regression of GCM-simulated height on a tropical SST time series obtained from the first EOF mode of re-analysis tropical diabatic heating. It is found that the results of all of these techniques agree extremely well with each other, and that the leading modes in the EOF (SVD) analyses explain large amounts of variance (squared covariance), about 50% (90%).

The spread of projections of individual seasonal means on the leading SVD mode of the seasonal-ensemble means, is less than the variation of the projection of the ensemble means on the SVD mode (90% significance level).

We draw two conclusions: first, that the GCM ensemble means simulate the observed anomalies with high accuracy; and second, that the observed and simulated anomalies are indeed forced by tropical diabatic heating.

The internal variability pattern was calculated in three different ways: (1) as the leading EOF of height of the deviations of each seasonal mean about the corresponding ensemble mean for that winter; (2) as the leading height EOF from the 39-year GCM integration forced by climatological (but annually varying) SST; and (3) as the leading height EOF from re-analyses for 29 winters not associated with very warm and cold tropical SSTs. The patterns derived from these analyses have a common structure. It is found that it is this internal variability pattern, and not the SST-forced pattern described above, that closely resembles the 'PNA' pattern of Wallace and Gutzler.

The SST-forced pattern in the GCM (characterized by the heterogeneous correlation pattern of the leading SVD mode for the ensemble means) is significantly different (95% confidence level) from the internal variability pattern (characterized by the homogeneous correlation pattern of the leading EOF of the GCM deviations about the ensemble mean) over a region in western North America and the adjoining eastern Pacific, a region north-east of the Great Lakes, and a small region in the Gulf of Alaska.

KEYWORDS: Ensemble prediction Predictability Seasonal forecasting

* Corresponding author: Center for Ocean–Land–Atmosphere Studies, 4041 Powder Mill Road, Suite 302, Calverton, MD 20705-3106, USA. e-mail: straus@cola.iges.org

1. INTRODUCTION

The paradigm of mid-latitude response to tropical variations of sea surface temperature (SST) is a confident one from the point of view of seasonal predictability, as the time-scale of SST variation is so long compared to that of the atmosphere. This ideal is best realized in the case of the strong winter mid-latitude response in the Pacific/North American region (PacNA) to tropical Pacific SST variations associated with the El Niño Southern Oscillation (ENSO) phenomenon (Bjerknes 1966, 1969; Horel and Wallace 1981; Hoskins and Karoly 1981; Simmons 1982; Shukla 1984). While both the nature of the tropical forcing and the dynamics of the remote response have been studied extensively, there is still a fundamental disagreement regarding the relationship of the remote response to the internal variability which occurs independently of the tropical SST forcing. This internal variability in the region of interest is dominated by the Pacific North American pattern (PNA), defined in terms of monthly mean teleconnection patterns (Wallace and Gutzler 1981) or in terms of leading rotated principal component analysis (Barnston and Livezey 1987). The PNA pattern, clearly shown in Fig. 17(c) of the former paper and Fig. 3(d) and (e) of the latter, is obtained from consideration of all winter months in the record, regardless of the state of the tropical Pacific SST. It is similar in some ways to the tropically forced ENSO response, as estimated (for example) in Zhang *et al.* 1996 (hereafter Z). However, the subtle structural differences between these two patterns (as emphasized by Z) are indicative of a different origin. In their coupled analysis of Pacific SSTs (tropical and mid latitude) with mid-latitude heights, Z show that by removing the influence of ENSO SST via linear regression, the remaining variability is dominated by the PNA pattern (compare their Figs. 5 and 6). The strong relationship of the PNA pattern to North Pacific extratropical SST anomalies, and the evidence that the latter represent the oceanic response to internal atmospheric variability, are reviewed in detail by Z.

However, another point of view interprets the ENSO mid-latitude response pattern as a natural mode of the atmosphere (usually taken to be represented by the PNA pattern) which has been excited by the tropical forcing, much as beating a drum excites its normal modes. What really distinguishes ENSO and non-ENSO winters in this view, is the strength and consistency (or probability) of the response, not its structure. This point of view has recently been expressed in modelling studies (Lau and Nath 1994; Lau 1997; Saravanan 1998), and from a more theoretical approach (Palmer 1993). Lau and Nath (1994) present the first coupled mode of the observed 'nearly global' SST field (40°S–60°N) with the northern hemisphere extratropical 500 hPa height field for 42 winters. The leading SST pattern encompasses not only tropical Pacific ENSO-like variability but also extensive variability in the North Pacific. The associated height pattern (their Fig. 3(a)) is similar to observational results presented by Z.

The general circulation model (GCM) simulation results of Lau and Nath (1994) are, however, difficult to interpret. The first coupled mode of the GCM integration using global SST variations prescribed from observations yields a pattern similar to the PNA pattern of Wallace and Gutzler (1981), while the first mode of the GCM integration using observed SST variations only in the tropics yields a different pattern, one much closer to the ENSO-related pattern diagnosed by Z and in many earlier studies (e.g. Horel and Wallace 1981; Ferranti *et al.* 1994; Graham *et al.* 1994; Kumar *et al.* 1996; and Chen and van Den Dool 1997). We note in this context, that the GCM response to ENSO is very weak in the GCM used by Lau and Nath (1994).

Saravanan (1998) shows evidence (his Fig. 1) that the regional wintertime variability of simulations made with either observed tropical or observed global SSTs is dominated by the same pattern which is seen in a long integration made with climatological

SSTs (i.e. SSTs having an annual cycle but no interannual variation). This pattern, obtained by regional empirical orthogonal function (EOF) analysis in each case, seems to resemble the PNA pattern more than the ENSO-response pattern seen by the studies quoted above*. Since in the case of the climatological SST run, the mode in question is seen only as the second EOF, it is not clear what role sampling errors may play here†.

The purpose of this paper is to use ensemble integrations by the atmospheric GCM of the Center for Ocean–Land–Atmosphere Studies (COLA) to assess the mid-latitude variability of seasonal means in the PacNA region due to ENSO-related SST variations for 16 recent winters (1981/82–96/97), and to contrast this SST-forced variability with chaotic internal variability both in terms of magnitude and characteristic patterns. The GCM is a critical tool because, unless assumptions are made, it is in general not possible from observations (analyses) alone to distinguish between the variability of seasonal means due to forcing by SST anomalies and the internal variability; the latter is due to the sensitivity of the nonlinear dynamics to initial conditions.

The GCM ensemble approach was designed to make this distinction possible. The idea is to integrate a GCM a number of times utilizing the same observed SSTs for a given season of a specific year, starting from different initial conditions. In this approach, the signal forced by the SST anomalies for that specific season is given approximately by the ensemble average of the individual seasonal means. This process tends to filter out the internal variability; in the limit of a very large ensemble size, this filtering is complete. The internal variability itself is estimated by the set of deviations of the individual seasonal means about the ensemble average. A collection of such ensembles for different calendar years (with distinct observed SSTs) allows for a general and robust estimation of SST-forced signal and of internal variability, if the ensemble size is large enough. A GCM ensemble of continuous multi-year integrations is an example of this approach, in which the initial conditions for a given season vary widely across members of the ensemble (see for example Lau and Nath 1994; Rowell *et al.* 1995; Rowell 1998). In this paper, the initial conditions for a given season are quite close to one another (and to the analysed atmospheric state) by design.

The validity of the ensemble approach is critically dependent upon at least two characteristics of the GCM: it must respond in a realistic manner to the dominant year-to-year SST variations of interest; and the overall variability of seasonal means in the GCM must be comparable to those in analyses. The COLA GCM satisfies these criteria quite well. The overall accuracy of the GCM in responding to fixed SST anomalies is assessed in a companion paper (Shukla *et al.* 2000; hereafter S) by comparing the anomalies of the ensemble means with analyses. Over the PacNA region the agreement is good, and it is outstanding during strong ENSO events. Note that while the comparison of the ensemble mean with analyses is useful when the SST-forced signal is large, it does ignore the role of internal fluctuations in the analyses. In terms of overall seasonal-mean variability in this region, the COLA GCM is also comparable to analyses, as we will show.

* Since the region used in the analysis of Saravanan does not extend to the east coast of North America, it is hard to make a precise comparison of this pattern with those found in other studies (e.g. Wallace and Gutzler 1981; Horel and Wallace 1981; Barnston and Livezey 1987).

† Although the difference in variance explained by the first and second EOFs in Saravanan (1998) is marginally significant, according to the test of North *et al.* (1982), no information is given about the significance of the difference between the second and third modes. Also, the constraint of orthogonality which is inherent in the analysis is especially restrictive when the spatial domain is limited.

The ensemble integrations of the COLA GCM (described in S) are used in conjunction with National Centers for Environmental Prediction (NCEP) re-analyses, hereafter referred to as 'observations'. Strictly speaking, the COLA integrations give an unambiguous depiction of the variability due to *global* SST variations vis-a-vis internal variability, as described above. We present evidence to show that during this period the ENSO-related SST signal is dominant in terms of its importance to mid-latitude height variations in the PacNA region. The role of the analyses in this paper is to verify the GCM, and to provide an observational estimate of ENSO- versus non-ENSO-related variability. The latter is obtained by contrasting a longer record of 29 winters in which ENSO-related SST (tropical Pacific) anomalies were absent with a record of ten winters in which these anomalies were strong. We show that the PacNA variability during non-ENSO winters from observations is quite similar to the internal GCM variability obtained from the deviations about the ensemble mean, thus suggesting that the importance of non-ENSO SST anomalies in forcing the PacNA region is quite small during winter. Finally, the variability of seasonal means in a 39-year continuous integration of the COLA GCM forced by climatological SSTs provides another estimate of the chaotic noise.

The GCM integrations and re-analysis datasets used are described in section 2. The overall magnitude of SST-forced and internal variability is discussed in section 3. Section 4 describes in detail the dominant patterns associated with SST-forced variability, and section 5 those associated with internal variability. Some salient points about the differences between these two patterns are highlighted in section 6. A summary is given in section 7, a discussion in section 8, and conclusions in section 9.

2. COLA GCM INTEGRATIONS AND DATA

(*a*) *DSP GCM integrations*

The Dynamical Seasonal Prediction (DSP) framework and the COLA GCM are described in detail in S. Briefly, the GCM is a global spectral model with horizontal rhomboidal 40 (R40) resolution, and 18 vertical levels. The prognostic variables are vorticity, divergence, virtual temperature, specific humidity, and logarithm of surface pressure. Prognostic cloud cover is used for the radiative transfer calculations. A realistic land surface model, realistic orography and a full, updated suite of physical parametrizations are included. In particular, the adoption of the relaxed Arakawa–Schubert convection scheme has greatly improved the simulation of the response to tropical SST variations (DeWitt 1996; DeWitt and Schneider 1999).

The GCM integrations consist of 16 ensembles, corresponding to the 16 winters of 1981/82 through 1996/97. The weekly observed Optimal Interpolation SST dataset for each winter was utilized (Reynolds and Smith 1994). Each ensemble consists of nine integrations started from the twice-daily sequence of analysed initial conditions from 0000 UTC 13 December through 0000 UTC 17 December. Each integration was continued until the end of March. Climatological soil moisture was used as an initial condition for the land surface model in each case, with the subsequent evolution of soil moisture being predicted. Unless otherwise stated, the definition of winter in this paper is the 100-day period starting at 0000 UTC 20 December.

(*b*) *Climatological SST integration*

The climatological integration, which used the same GCM as in the DSP integrations, was initialized from the National Meteorological Center (NMC) analysis valid for 0000 UTC 1 January 1977, with climatological soil moisture, and was integrated for 39

years. The prescribed SSTs used as boundary conditions possess the annual cycle seen in observations, but have no interannual variability; each month's SST was obtained as a climatological average from Reynolds (1988).

(c) *NCEP re-analyses (observations) and GCM data*

The re-analyses of the NCEP (Kalnay *et al.* 1996) were obtained from the archive at the National Center for Atmospheric Research, for the 39 winters 1958/59 through 1996/97. The 500 hPa height field was interpolated from the original 2.5° × 2.5° grid to a 4° × 5° (latitude × longitude) grid, and was further interpolated to an equal-area grid (Molteni *et al.* 1988) extending over the PacNA region (defined to be 150°E–30°W, 20–80°N) for the EOF and singular-value decomposition (SVD) analyses in sections 4–6. The total diabatic heating rates used in the SVD analysis were obtained on the grid of the re-analysis forecast model T62 horizontal Gaussian grid (192 × 94 grid points). The original 28 levels of diabatic heating were *vertically integrated* (not averaged) into six layers, with mid points approximately equally spaced between 1000 hPa and 100 hPa. For the SVD analysis, the 6-layer heating was interpolated to a 5° × 5° grid extending over the Pacific tropical region (120°E–80°W, 20°S–20°N). Throughout this paper, the height, wind and heating data from the re-analyses are referred to (for convenience) as *observations*.

The GCM data are all originally on the R40 Gaussian grid (128 × 102 grid points) with 18 levels in the vertical. For the EOF and other analyses in sections 4–6, the 500 hPa height fields are interpolated first to a 4° × 5° (latitude × longitude) grid and further interpolated to an equal-area grid over the PacNA region in the same manner as the observations. The diabatic heating fields are first vertically integrated over six layers (as with the observations), and then interpolated to a 5° × 5° grid extending over the Pacific tropical region.

(d) *SST datasets*

In order to have a definition of strong warm and cold ENSO events, which we collectively refer to as strong ENSO events, the Niño-3 SST anomaly index*, averaged for the three-month period of January to March, was computed from the first version (1.1) of the global sea ice and SST (GISST) dataset (Parker *et al.* 1995) for the 39 winters 1958/59 through 1996/97. The five strongest warm events (positive Niño-3 anomaly) are the winters of 1965/66, 1972/73, 1982/83, 1986/87 and 1991/92. The five strongest cold events (negative Niño-3 anomaly) are the winters of 1970/71, 1973/74, 1975/76, 1984/85 and 1988/89. The 29 winters which exclude these 10 winters are referred to as normal, or non-ENSO winters.

(e) *Nomenclature*

In order to distinguish the many datasets, from observations and from the GCM, that are used in this paper, it is useful to define the following nomenclature for seasonal means:

- **OBS 16** refers to the seasonal means for the 16 winters of 1981/82 through 1996/97 from the observations (NCEP re-analyses) which correspond to the DSP period.
- **OBS 39** refers to the seasonal means for all 39 winters 1958/59 through 1996/97 from the observations (NCEP re-analyses).

* The Niño3 index is defined as the average SST anomaly in the region 30–90°W, 5°S–5°N.

• **OBS 10** refers to the seasonal means for the subset of 10 winters from OBS 39 that include all strong ENSO events (see previous subsection).

• **OBS 29** refers to the seasonal means for the subset of 29 winters from OBS 39 that *exclude* all strong ENSO events (see previous subsection). These are the non-ENSO winters.

• **GCM 16** refers to the *ensemble average* of GCM seasonal means for the 16 winters of 1981/82 through 1996/97.

• **GCM 16×9** refers to *all* 144 GCM seasonal means, that is nine seasonal means for each of the 16 winters of 1981/82 through 1996/97.

• **GCM D 16×9** refers to the *deviations* of GCM seasonal means about the ensemble average for the nine ensemble members for each of 16 winters of 1981/82 through 1996/97.

• **GCM Cli-SST** refers to the 39 seasonal means from the GCM integration using climatological SSTs.

3. SST-FORCED AND INTERNAL VARIABILITY: OVERALL MAGNITUDE

In this section the overall variability of seasonal means in the GCM and the corresponding observations are compared, as well as the variability that can be ascribed to ENSO SST forcing and that due to internal variability. The total GCM variance and the GCM variance due to SST forcing are calculated in a manner which takes into account the finite size of the ensemble (Rowell *et al.* 1995), as detailed in the appendix. The variance of observed seasonal means for the 16 winters 1982/83–96/97 (dataset OBS 16) is compared with the total GCM variance from the GCM-16×9 dataset in Fig. 1. The GCM variance here is defined as $V_{TOT} = V_{SST} + V_e$, where $V_{SST} = V_{EM} - (1/n)V_e$, with V_{EM} the variance of the ensemble mean, V_e the variance of deviations about the ensemble mean, and n the number of members in the ensemble for each year; (see the appendix). The strong Pacific maximum near 160°W and 45°N is well simulated in Fig. 1, as is the broad band of high variance over Canada. The major difference occurs just over the western coast of Canada, where the model over-predicts the variance.

Estimates of the internal variability are given in Fig. 2 which shows the variance of the GCM from (a) the GCM-D16×9 and (b) GCM-Cli-SST datasets. These purely internal variances are compared to (c) the OBS-29 variance. The two GCM estimates of internal variability are very similar. However there are differences with the observed non-ENSO variance: the distinct observed North Pacific maximum is weaker (but broader) in the GCM. This difference is due both to unrealistic behaviour in the GCM and to SST variations not related to ENSO, which contribute to the observed variance. We cannot separate these effects.

The variances shown in Figs. 1 and 2, as well as all further results to be shown in this paper, were calculated after removing the North Atlantic/Arctic oscillation in the 500 hPa height field from both the observational and model datasets. This oscillation is hemispheric and is fairly similar in its manifestations in the GCM and the observations. It is also strongly related to the annular mode discussed by Thompson and Wallace (2000). Details relating to the North Atlantic/Arctic oscillation and its removal from the various datasets are given in the appendix.

The ratio of the SST-forced variance to internal variance can be tested for statistical significance according to standard analysis-of-variance methods (Scheffé 1959; Rowell 1998). The ratio, shown in Fig. 3(a), exceeds 3.0 in the eastern Pacific and is even larger

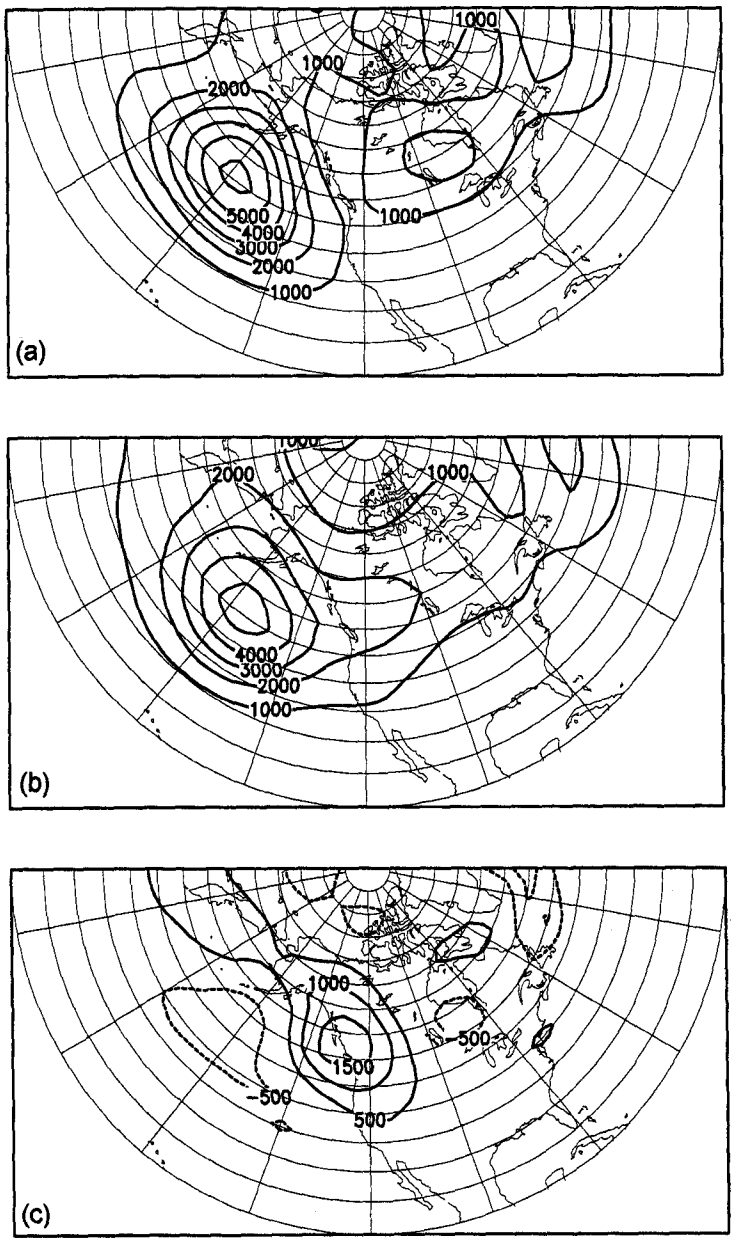

Figure 1. Variance of winter mean 500 hPa height in the region 150°E–30°W, 20–85°N. The North Atlantic/Arctic oscillation has been removed. (a) From OBS 16 (re-analyses for 16 winters 1981/82–96/97); (b) from GCM 16 × 9 (all GCM integrations). (c) Difference (b) minus (a). The contour intervals are 1000 m^2 in (a) and (b), and 500 m^2 in (c) where dashed lines are negative. See text for details.

over Mexico. The corresponding F statistic* (Fig. 3(b)) is given basically by the ratio of the SST-forced variance to its uncertainty due to the presence of internal noise. Values of F greater than 2.19 (which corresponds to 99% statistical significance) in Fig. 3(b)

* The F statistic is defined here as $F = (1 + nV_{SST}/V_e)$, where n is the ensemble size ($n = 9$), V_{SST} the SST forced variance and V_e the internal variance (see Scheffé 1959, p. 226).

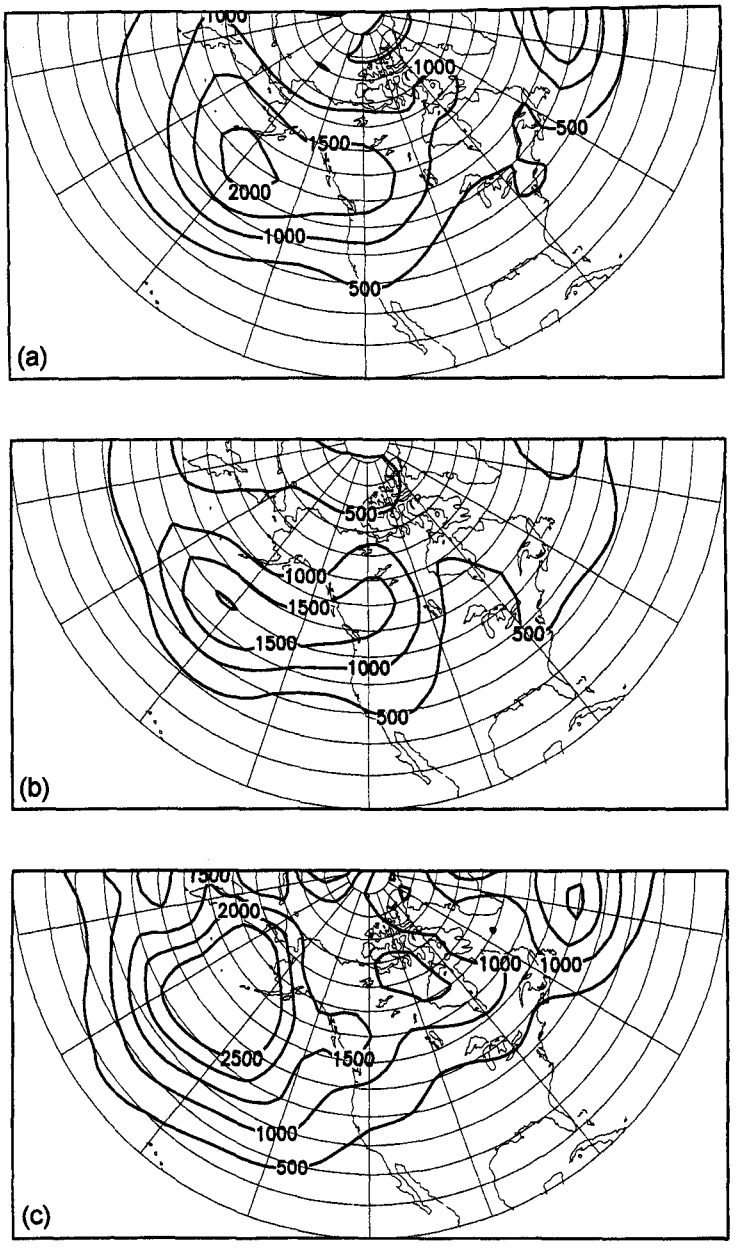

Figure 2. Variance of winter mean 500 hPa height for: (a) GCM D16×9 (seasonal mean deviations about the ensemble mean; (b) GCM Cli-SST (39 winters from the GCM integration using climatological SST); (c) OBS 29 (re-analyses for the 29 non-ENSO winters). The North Atlantic/Arctic oscillation has been removed. The contour intervals are 1000 m^2. See text for details.

indicate rejection of the null hypothesis that the SST-forced and internal variances are equal, at a 99% confidence level. Clearly the null hypothesis is rejected over almost the entire region, with the SST-forced variance exceeding the internal variance.

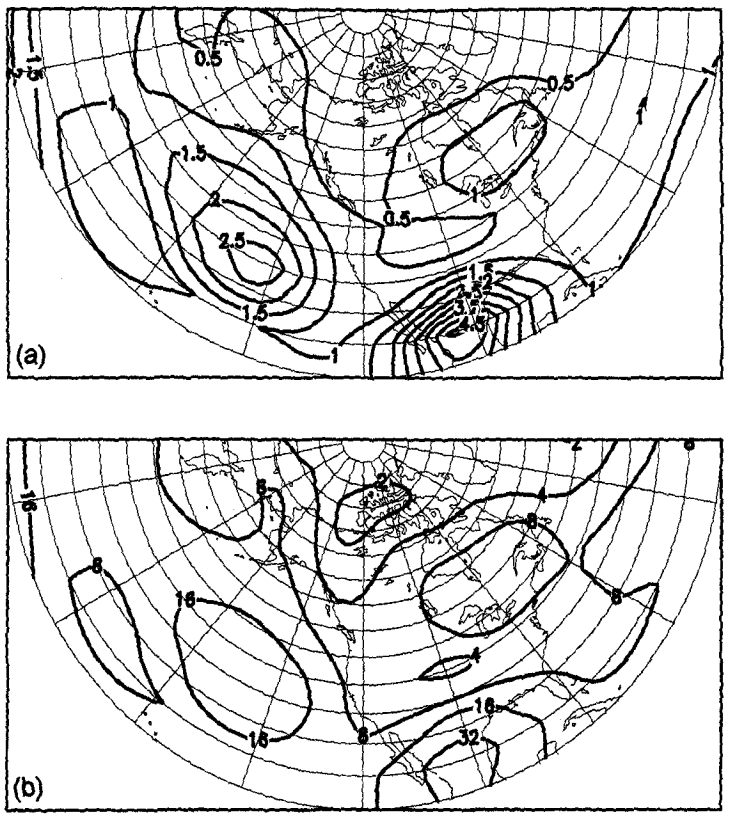

Figure 3. (a) Ratio of the SST-forced variance, V_{SST}, to the internal variance, V_e, (variance of GCM D 16×9, the seasonal-mean deviations about the ensemble mean). The North Atlantic/Arctic oscillation has been removed. (b) The corresponding F statistic defined as $F = (1 + nV_{SST}/V_e)$, where n is the ensemble size ($n = 9$), (Scheffé 1959, p. 226). $F = 2.19$ corresponds to 99% statistical significance. See text for details.

4. SST-FORCED VARIABILITY: DOMINANT PATTERN

(a) *GCM ensemble mean results*

In order to determine the dominant patterns associated with the SST forcing, we employ EOF analysis of the 500 hPa height of GCM 16 restricted to the PacNA region. The grid utilized is discussed in section 2. Since the leading hemispheric EOF has been removed (see section 2 and the appendix), there is no need to rotate these regional EOF modes in order to achieve stable, localized patterns. In fact, Table 1 gives the explained variance and associated uncertainty (North *et al.* 1982) of the first two regional EOF modes for the GCM-16 dataset. It is clear that the first mode, explaining 59% of the spatially integrated variance, dominates the spectrum. The uncertainty in the percentage of explained variance (North *et al.* 1982) gives an indication of the sampling error. Since this uncertainty is less than the difference in explained variance between the first two modes (see Table 1), the distinction between them is statistically significant.

The homogeneous correlation height pattern associated with the first mode, EOF-1, is given in Fig. 4(a). This is defined as the temporal correlation of the variation of the height field at each grid point with the variation of the time series (principle component) associated with the first mode (Bretherton *et al.* 1992). The pattern consists of broad centres in the mid-latitude (45°N) Pacific between 140°W and 160°E, between (and

TABLE 1. ENSO-FORCED VARIABILITY

Dataset	EOF-1% var EOF-2% var	EOF-1 exp var	SVD-1% sqcov SVD-2% sqcov	SVD-1 exp cov
OBS 10	57 (25) 14 (6)	657	90 5	207
OBS 16	51 (18) 15 (5)	534	88 5	135
GCM 16	59 (20) 15 (5)	325	86 8	182

Datasets are defined in subsection 2(e).
% var is the percentage variance explained by the given EOF; numbers in parentheses give the uncertainty, as in North *et al.* (1982).
exp var is the actual explained variance (m^2) averaged over PacNA.
% sqcov gives the percentage of squared covariance, P, explained by the given SVD; where the total squared covariance is given by $\sum_m \sum_n \langle h_m Z_n \rangle^2$. Here h_m refers to the heating anomaly at point m, Z_n to the height anomaly at point n, and the angular brackets a time/sample mean.
exp cov gives the actual explained covariance (W m^{-1}) averaged over PacNA, given by $\{P \sum_m \sum_n \langle h_m Z_n \rangle^2/(MN)\}^{1/2}$, where M and N are total numbers of points.

just west of) the Great Lakes and Hudson bay, and over the Gulf of Mexico (near 30°N) extending across Florida eastward into the Atlantic. It strongly resembles the correlation of SST with 700 hPa height presented by Horel and Wallace (1981, their Fig. 9(a)), and the ENSO warm-event composites of Kumar *et al.* (1996, their Fig. 5(a)), and Chen and van Den Dool (1997, their Fig. 3).

In order to establish a connection between major fluctuations of the GCM-16 tropical Pacific diabatic heating field and the 500 hPa height field for the PacNA region, we have also carried out an SVD analysis of these two fields (see section 2 for details of the regions and grids). The SVD technique identifies modes in a pair of fields which maximize the (squared) covariance between the fields (Bretherton *et al.* 1992). We have chosen to use the three-dimensional tropical diabatic heating, rather than the (more conventional) SST anomaly field in the SVD analysis for two reasons. Firstly, it is the diabatic heating and the associated changes in tropical circulation that are directly responsible for the Rossby wave-train response into mid latitudes (Hoskins and Karoly 1981; Sardeshmukh and Hoskins 1988); the SST anomaly will only be effective if it can create a suitable diabatic heating anomaly. Secondly, we wish to diagnose the three-dimensional structure of the diabatic heating anomaly that is associated with ENSO. The price that we pay for this choice is that, in the case of the 'observations', the diabatic heating does not in fact come from observations, but directly from the numerical forecast model.

The squared covariance explained by the first two SVD modes for the GCM-16 data is given in Table 1. Again, the first mode (explaining 86%) dominates the second (explaining 8%). The normalized explained squared covariance (which tends to be more robust statistically, see Wallace *et al.* 1993) is also given for the first mode in Table 2. The spatial structure of the 500 hPa height component of the first SVD is given by the heterogeneous correlation, which is defined as the temporal correlation of the height-field variation at each grid point with the leading SVD tropical heating time series (SVD1). The heterogeneous correlation, shown in Fig. 4(b), is nearly identical to the pattern associated with the first EOF (Fig. 4(a)). Fig. 4(c) is discussed later.

The three-dimensional GCM-16 tropical Pacific diabatic heating pattern which is associated with SVD-1 is shown in Fig. 5, which has been scaled so that the time coefficient associated with this mode is 1.0 for the winter of 1982/83. Vertically

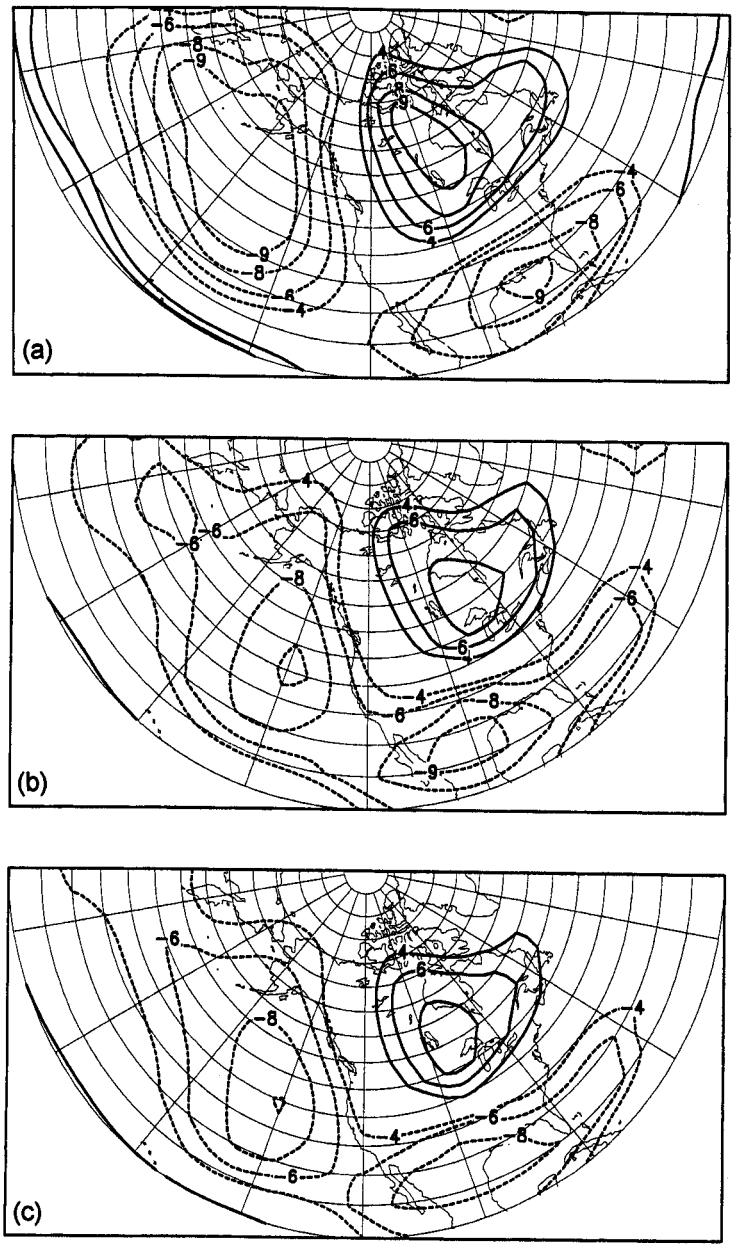

Figure 4. Correlations of 500 hPa height from GCM 16 (ensemble seasonal means for 16 winters): (a) homogeneous correlation of EOF-1; (b) heterogeneous correlation of SVD-1 coupling the height field with tropical Pacific diabatic heating field; (c) external correlation with tropical Pacific diabatic heating time series derived from a 39-winter SVD analysis of OBS 39 (NCEP re-analyses). All correlations have been multiplied by 10. The contour interval is 2, with the zero contour omitted, and an added contour inserted at the value of 9.0. See text for further details.

integrated, it consists of equatorial heating centred at the date-line, with cooling in a surrounding horse-shoe shaped region.

The heating indicates an enhancement of precipitation in both the intertropical Pacific convergence zone and the South Pacific convergence zone, in agreement with the

TABLE 2. SVD CALCULATIONS (LEADING MODES)

Dataset	Total SqCov	Expl. Sq Cov	Norm Sq Cov	Norm Ex SqCov
OBS 10	2.48×10^{10}	2.23×10^{10}	0.53	0.51
OBS 16	1.08×10^{10}	0.95×10^{10}	0.43	0.40
GCM 16	2.01×10^{10}	1.73×10^{10}	0.43	0.40

Total SqCov is the total squared covariance summed over all grid points (W m^{-1}) given by $\sum_m \sum_n \langle h_m Z_n \rangle^2$, where h_m is the heating anomaly at grid point m, Z_n the height anomaly at point n, and the angular brackets denote a time/sample mean.
Expl. SqCov is P $\sum_m \sum_n \langle h_m Z_n \rangle^2$, where P is the percentage of explained squared covariance given in Table 1.
Norm. Sq Cov is given by $(\sum_m \sum_n \langle h_m Z_n \rangle^2 / V_h V_z)^{1/2}$, where $V_h = \sum_m \langle h_m h_m \rangle$ and $V_Z = \sum_n \langle Z_n Z_n \rangle$ (see Wallace *et al.* 1993).
Norm. Ex. Sq Cov is given by $(P \sum_m \sum_n \langle h_m Z_n \rangle^2 / V_h V_z)^{1/2}$ (see Wallace *et al.* 1993).

ENSO-related variations of precipitation estimated from outgoing long-wave radiation, and from the microwave sounding unit satellite data (Yualeve and Wallace 1994; Straus and Shukla 1997). The maximum cooling at about 15°N, 150°E lies somewhat to the east of the observed suppression of precipitation in the above studies. The vertical structure of the GCM heating, with a maximum at 500 hPa, is distinct from that shown in the GCM study of Straus and Shukla (1997), who found a maximum at 300 hPa. In that study, the GCM utilized a very different parametrization scheme for cumulus convection.

This three-dimensional structure is the same as that of the first EOF of GCM-16 tropical diabatic heating alone, also shown in Fig. 5 and scaled in the same manner as above. The first mode, which explains 42% of the total variance, dominates all other modes; the second EOF explains only 20% of the variance.

Clearly the dominant SVD patterns of tropical heating and mid-latitude height capture the dominant patterns present in each field separately, putting to rest any concern that the relatively small number of independent maps in the GCM-16 dataset leads to severe sampling problems. That these dominant patterns are related specifically to ENSO is demonstrated in Fig. 6(a), which gives the time series associated with both EOF-1 (solid curve) and SVD-1 (dashed curve) modes for the GCM. These time series are standardized to have zero mean and unit variance. Very sharp maxima of both time series occur for the winters of 1982/83, 1986/87, and 1991/92, corresponding to warm winters as defined from the GISST (see section 2). The cold events of 1984/85 and 1988/89 lie in (separate) minima of the time series which, however, also encompasses the non-ENSO winters of 1983/84 and 1989/90. After 1991/92, the fluctuations are weaker. (We defer until later a discussion of the differences between the GCM time series and the dotted and dash-dot curves in Fig. 6(a), derived from observations.) The diabatic heating time series for the GCM ensemble-mean EOF and SVD modes, shown in Fig. 6(b), behave in a similar manner. Here the warm events are marked by larger amplitudes than the cold events, which are not well distinguished from other winters.

We have chosen to utilize tropical diabatic heating as opposed to SST anomalies in the SVD analysis. However, a comparison of the results in Figs. 4–6 with the corresponding SVD results for height and SST anomalies given in S indicates nearly identical height patterns. The maximum in the SST pattern associated with the first SVD mode in S is shifted considerably to the east compared to the corresponding diabatic heating maximum shown here. This is a reflection of the fact that it is the total SST field, and not its anomaly, that influences convection and diabatic heating so that, while

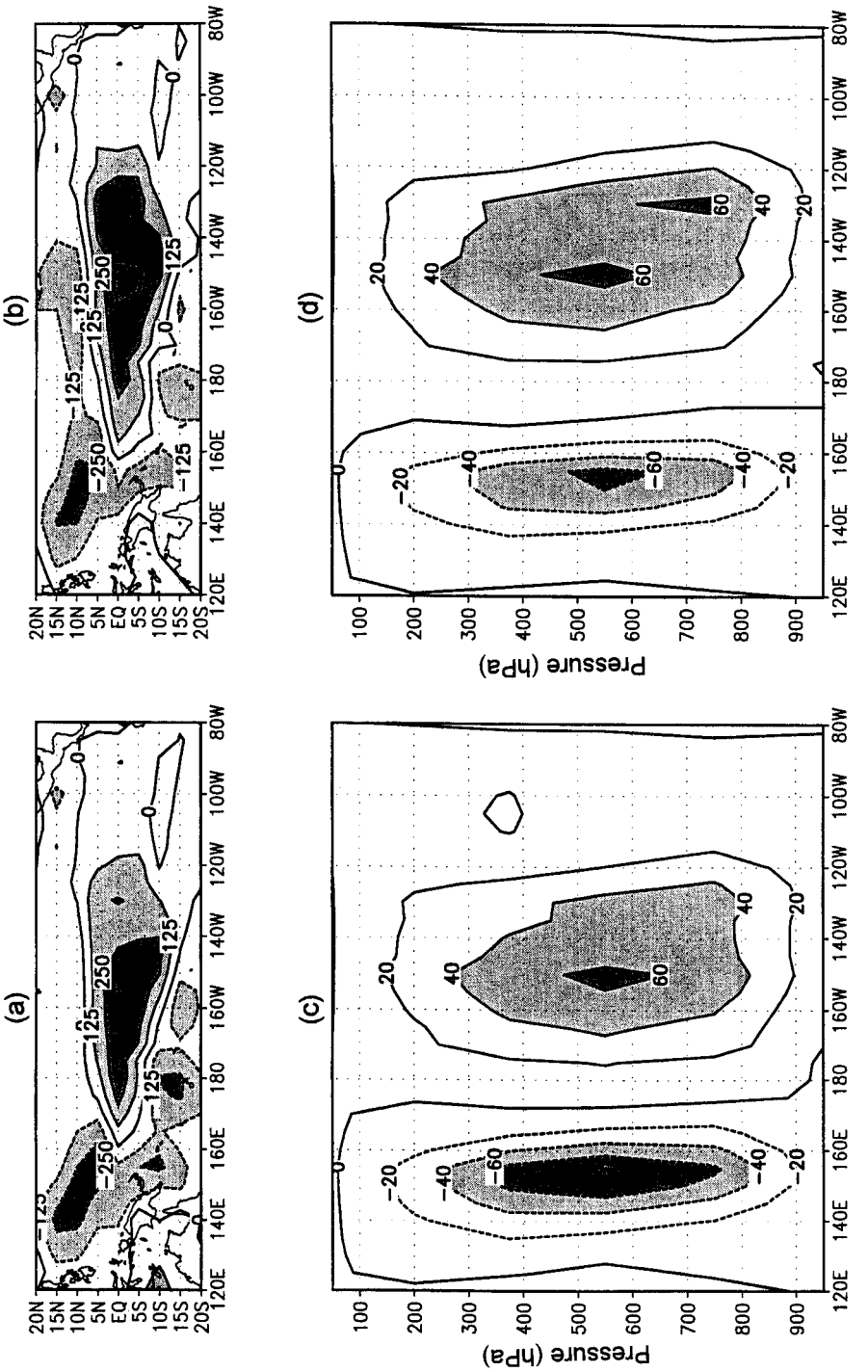

Figure 5. Tropical Pacific diabatic heating fields from GCM 16 (ensemble seasonal means for 16 winters): (a) vertically integrated diabatic heating from EOF-1; (b) vertically integrated diabatic heating from SVD-1 of 500 hPa height coupled with heating; (c) longitude/pressure section (averaged 10°S–10°N) of EOF-1; (d) longitude/pressure section (averaged 10°S–10°N) from SVD-1. The contour interval is 125 W m^{-2} in (a) and (b), and 20 W m^{-2} in (c) and (d). Fields are normalized so that the associated EOF (or SVD) principal components have a value of +1.0 for the winter of 1982/83. See text for details.

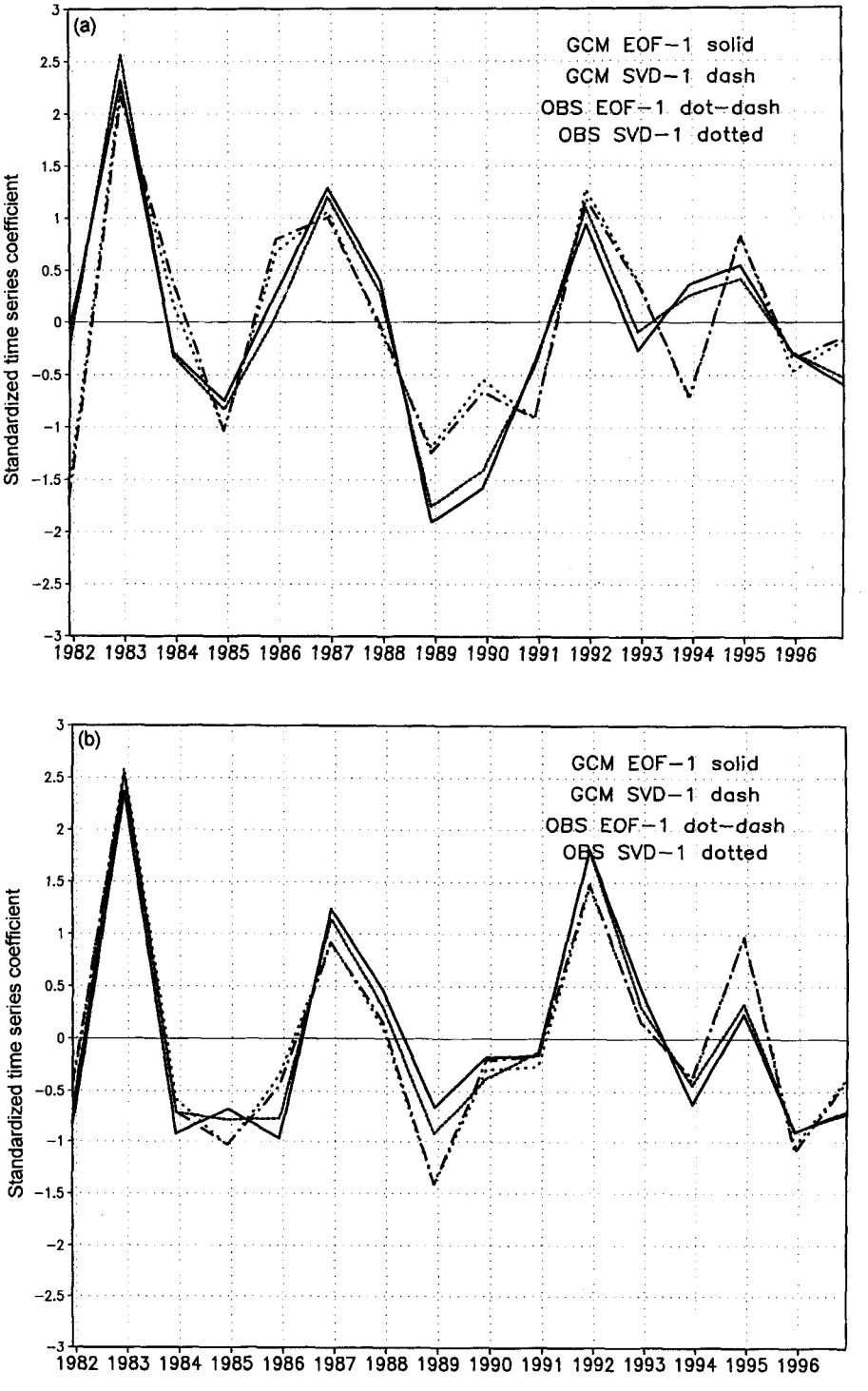

Figure 6. (a) Time series (principal components) of 500 hPa height associated with EOF-1 (SVD-1) of GCM 16, given by the solid (short-dashed) lines. Also shown are the time series of 500 hPa height associated with EOF-1 (SVD-1) of OBS 16, given by the dot-dashed (dotted) lines. All time series are standardized to have zero mean and a standard deviation of 1.0. (b) As (a) but for time series of tropical Pacific diabatic heating. See text for details.

the largest ENSO SST anomalies lie in the eastern tropical Pacific, the warmest water extends eastwards only to the central Pacific (Desser and Wallace 1990).

In order to demonstrate that the leading height pattern in the PacNA region shown in Fig. 4(a) and (b) is not very sensitive to the particular 16 winters chosen, we have carried out an EOF analysis of tropical Pacific diabatic heating from the longer OBS 39 (re-analysis) dataset. The time coefficients of the leading EOF mode provided an independent extended time series, with the last 16 winters corresponding to those of the GCM 16 dataset. The temporal correlation of the GCM 16 height at each grid point with the corresponding portion of this extended time series is shown in Fig. 4(c). The pattern closely resembles that shown in Fig. 4(a) and (b).

In order to demonstrate further that the leading SVD mode of the ensemble mean captures the SST-forced signal, we have projected each of the 144 GCM integrations (GCM 16×9) onto this mode. For each of the 16 years, the individual ensemble members' projection coefficients (principal components) are shown in Fig. 7(a) as open circles, and their mean (which is the same as the projection coefficient of the ensemble-mean height) as the solid curve (identical except for scaling to the solid curve of Fig. 6(a)). The spread of the ensemble is measured by the variance of the projections about the mean for each year. This intra-ensemble variance is plotted as the heavy solid curve in Fig. 7(b), and the average of that variance over the 16 years is given by the light dashed line. The ratio of the variance of the ensemble-mean projections (given by the light solid line in Fig. 7(b)) to the average intra-ensemble variance, is a measure of the dominance of the SST-forced signal over the noise due to initial-condition dependency. The value of 2.48 obtained for this ratio is significant at the 90% level using a one-sided F test. Thus the dominance of SST signal to internal variability seen in the total field (Fig. 3) is preserved by this dominant SVD mode. (We have repeated this calculation using projections onto the leading EOF; the variance ratio is 2.18, which is not significant at the 90% level.)

(*b*) *Observations*

We have carried out similar EOF and SVD calculations for the observed seasonal means for both the corresponding 16-winter period (OBS-16 dataset), and for the 10 winters deemed strong ENSO events in section 2 (OBS-10 dataset). The single record of 16 winters contains a number of strong ENSO events, but non-ENSO SST fluctuations are also present. By repeating the analysis using only the 10 strong events we try to gauge their effect. For the 16-winter period, the EOF-1 explained 51% of the variance (see Table 1), and dominates that explained by EOF-2 (15%); the explained squared covariance of 88% is also much larger than the 5% explained by the second mode. These statistics are quite similar to those for the GCM 16 and the OBS-10 datasets.

The actual (area-averaged) height variance explained by EOF-1 for the GCM 16 results (3.25×10^2 m^2, see Table 1) is only 61% of the height variance explained in the observations (5.34×10^2 m^2). This is a reflection of the greater total variance of the observed seasonal means compared to that of the ensemble-mean GCM seasonal means. The observed variance contains contributions due both to internal (non SST-related) variability and to non-ENSO SST-forced variability, while the internal variations have been partially filtered out in the GCM-ensemble seasonal means.

The mid-latitude height EOF-1 homogeneous correlation patterns and SVD-1 heterogeneous correlations patterns are presented in Fig. 8 for OBS-16 and OBS-10 datasets, while the corresponding (vertically integrated) diabatic heating maps are given in Fig. 9. The agreement between the two (overlapping) observed datasets, and between

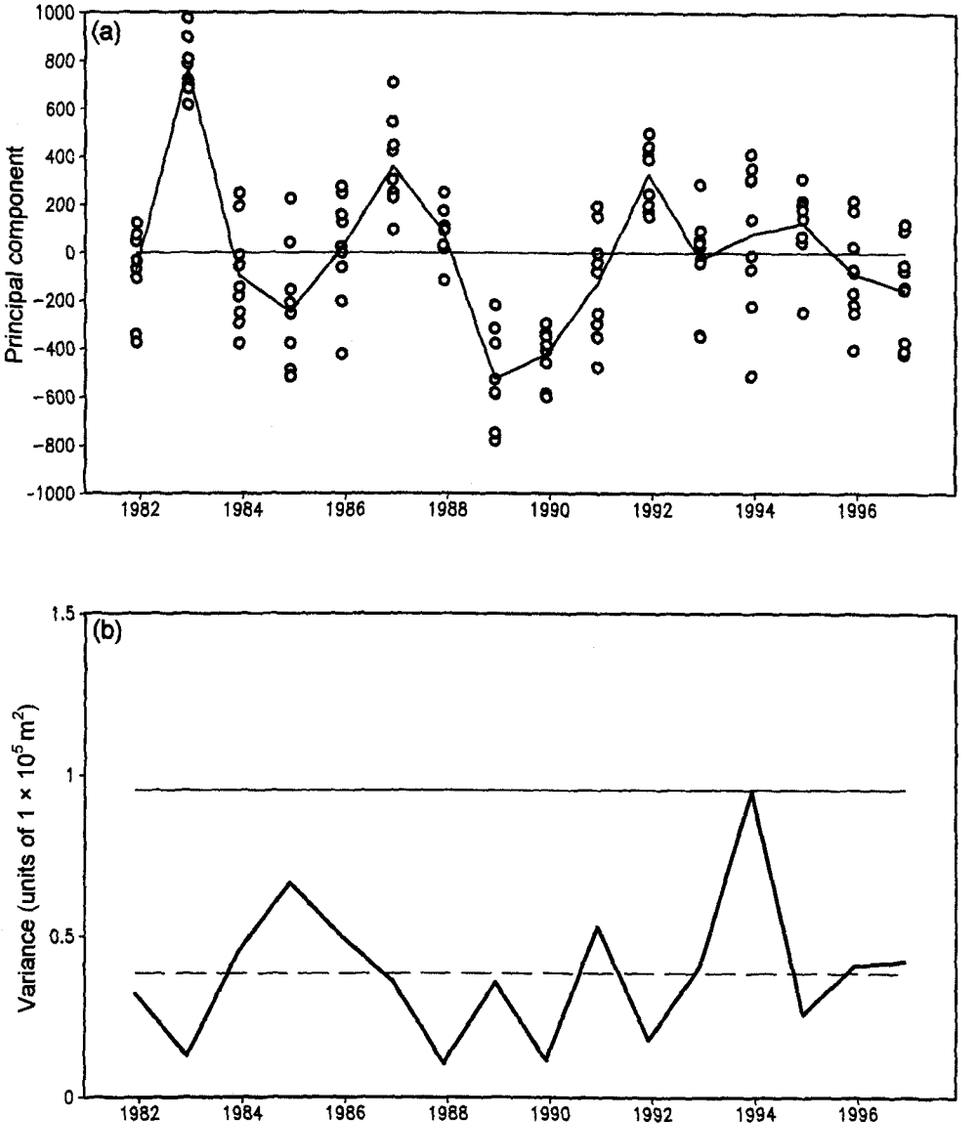

Figure 7. (a) Projection of 16 GCM ensemble means on SVD-1 (solid line), and projections of each individual GCM seasonal mean on the same leading SVD mode (given by the open circles). (b) The thick curve gives the variance of the individual projections (open circles in (a)) about the ensemble mean, as a function of winter. The thin horizontal solid line gives the overall variance of seasonal-ensemble means (curve in (a)), and the thin horizontal dashed line the variance of the individual projections averaged over winters. The ratio of the former to the latter (F value) is 2.48, significant at the 90% confidence level. See text for further details.

observations and the GCM 16 (Figs. 4 and 5) is quite remarkable. A subtle shift in the positive height maximum over Canada some 5°–10° west is noted in the observations compared to the GCM-ensemble mean, as is the presence of a separate maximum over the north-western Atlantic. Not only do the height patterns for both EOF and SVD modes, and for both OBS and GCM datasets, resemble those found by Horel and Wallace (1981), Kumar *et al.* (1996), and Chen and van Den Dool (1997) as mentioned

TABLE 3. INTERNAL VARIABILITY

Dataset	EOF-1% var EOF-2% var	EOF-1 exp var
OBS 29	35 (9) 18 (5)	326
GCM D 16×9	28 (3) 14 (2)	417
GCM CLI-SST	33 (7) 20 (5)	208

See Table 1 for explanation of column headings.

above, but they are also in substantial agreement with the leading canonical mode between observed tropical SSTs and northern hemisphere 700 hPa heights presented in Fig. 1(d) of Graham, *et al.* (1994), and with the GCM response to ENSO SST forcing simulated by Ferranti *et al.* 1994 (their Fig. 12).

The (normalized) height time series associated with the leading EOF and SVD modes in the OBS 16 are given by the dot-dash and dotted lines in Fig. 6(a), while the corresponding heating time series are given in Fig. 6(b). In all cases the three warm ENSO winters of 1982/83, 1986/87 and 1991/92 are marked by sharp maxima, but the cold events are not always marked by sharp minima, e.g. 1984/85 (1988/89) in the heating (height) time series. In addition, a large negative value of the height time series is seen in 1981/82, and to a certain extent in 1990/91, both non-ENSO winters. Differences between the observed and GCM time series in Fig. 6(a) are smallest during warm events, but are not small at other times (1981/82, 1989/90, 1993/94). Although this record of leading modes obtained from the observations is dominated by ENSO-related variations, evidence of variability not related to ENSO is also seen.

5. INTERNAL VARIABILITY

In this section we estimate the dominant patterns associated with variability not forced by SST variations, by examining deviations from the ensemble mean in the GCM experiments (GCM D16×9) and 39 years of the climatological-SST GCM run (GCM Cli-SST). In addition, the observed 29 winters not considered to be ENSO events (OBS 29) are analysed, although this record also includes variability forced by non ENSO-related SST fluctuations.

The homogeneous correlation patterns for the first EOF of the three datasets are shown in Fig. 10. The percentage of explained variance of the first two EOFs are given for each dataset in Table 3. Even though the leading EOF explains a modest fraction of the variance (28% to 35%), it is significantly different from the second EOF in each dataset. These patterns are fairly close to the classic 'PNA' pattern obtained by Wallace and Gutzler (1981, hereafter WG) on the basis of teleconnection analysis, as shown in their Figs. 16(a)–(d) and 17(c). The results of a teleconnection analysis carried out on the three datasets discussed above, yields patterns which are similar to the homogeneous correlation patterns of Fig. 10. Our internal variability patterns also resemble the EOF composite presented by Lau (1997) for his control run, in which SSTs varied climatologically (his Fig. 5).

6. COMPARISON BETWEEN SST-FORCED AND INTERNAL VARIABILITY PATTERNS

In this section we focus on the significance of the differences between the two distinct patterns that have emerged from the analysis of this paper. The heterogeneous

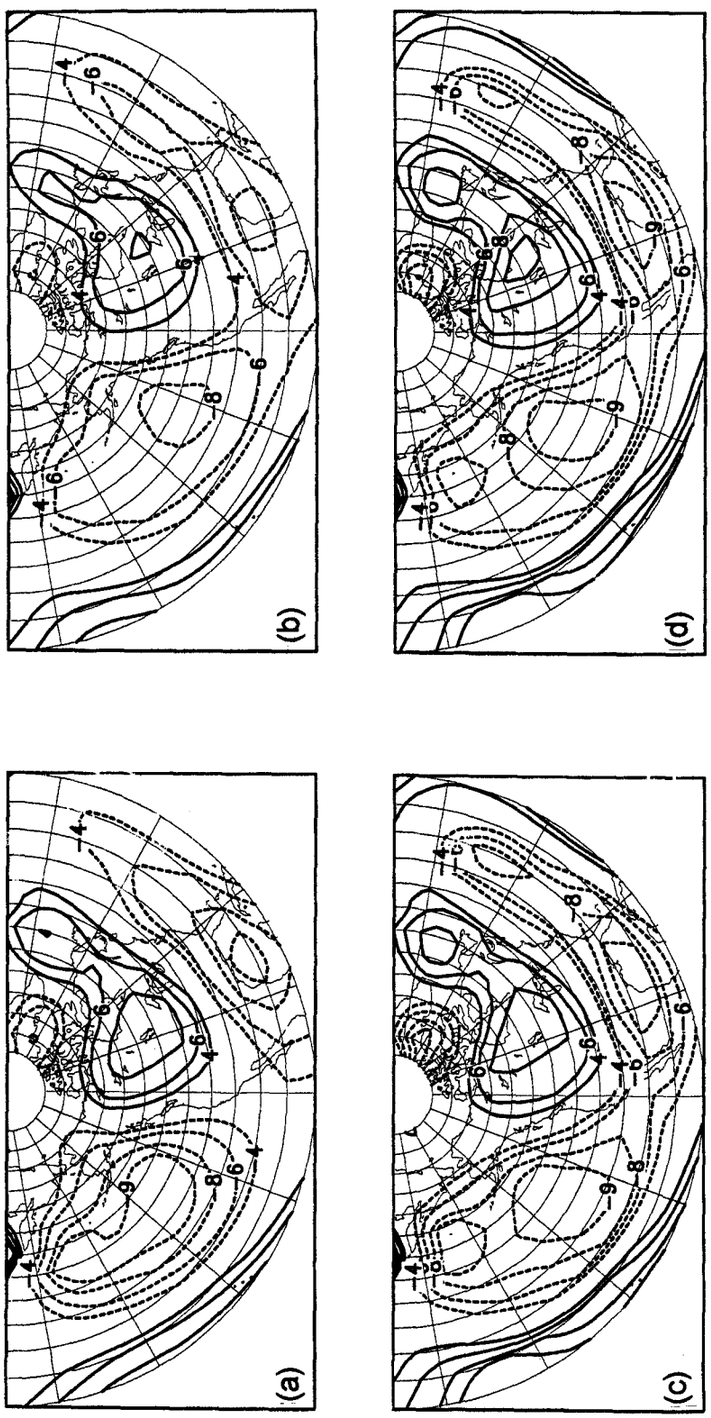

Figure 8. Correlations of 500 hPa height from OBS 16 (NCEP re-analyses). (a) Homogeneous correlation of EOF-1 for 16 winters (1981/82–1996/97). (b) Heterogeneous correlation of SVD-1 coupling the height field with tropical Pacific diabatic heating for the same 16 winters. (c) Homogeneous correlation of EOF-1 from OBS 10 (strong ENSO winters). (d) Heterogeneous correlation of SVD-1 coupling the height field with tropical Pacific diabatic heating for the same 10 strong ENSO winters. All correlations have been multiplied by 10. The contour interval is 2, with the zero contour omitted, and a contour at 9.0 added. See text for details.

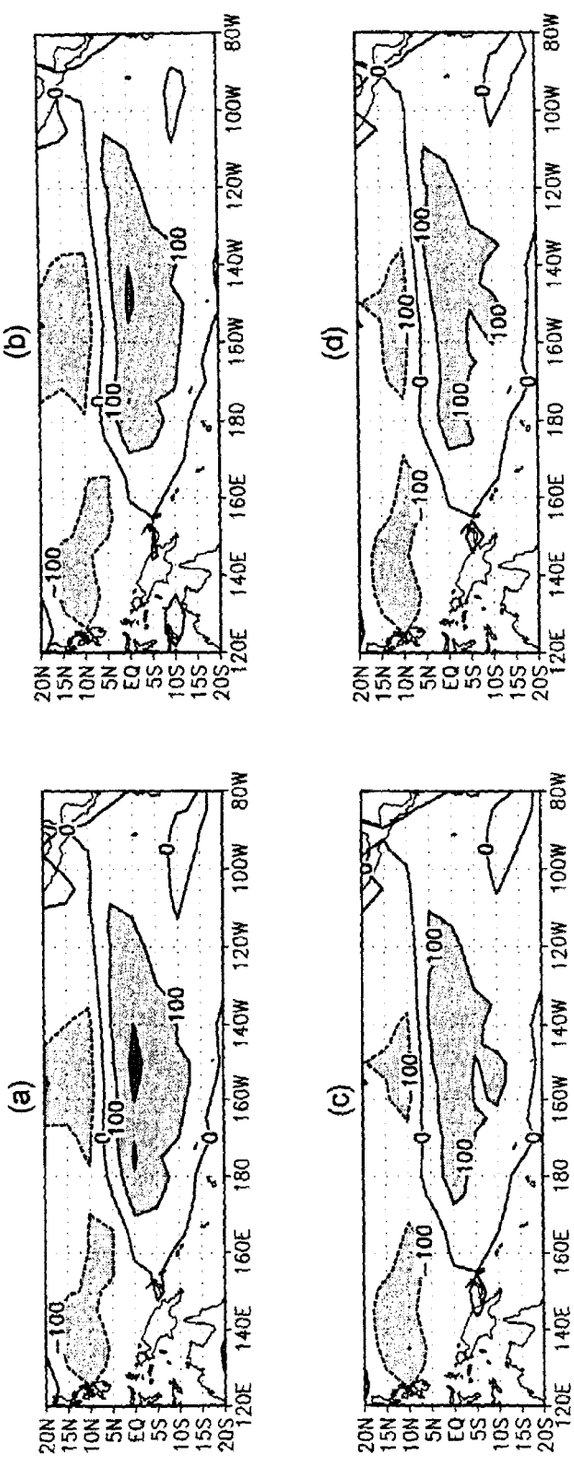

Figure 9. Vertically integrated tropical Pacific diabatic heating fields from NCEP re-analyses: (a) from EOF-1 for 16 winters (1981/82–1996/97); (b) from SVD-1 of 500 hPa height coupled with heating for the same 16 winters; (c) from EOF-1 for 10 strong ENSO winters; (d) from SVD-1 for the same 10 strong ENSO winters. The contour interval is 100 W m^{-2}. Fields are normalized so that the associated EOF (or SVD) time series have a value of +1.0 for the winter of 1982/83. See text for details.

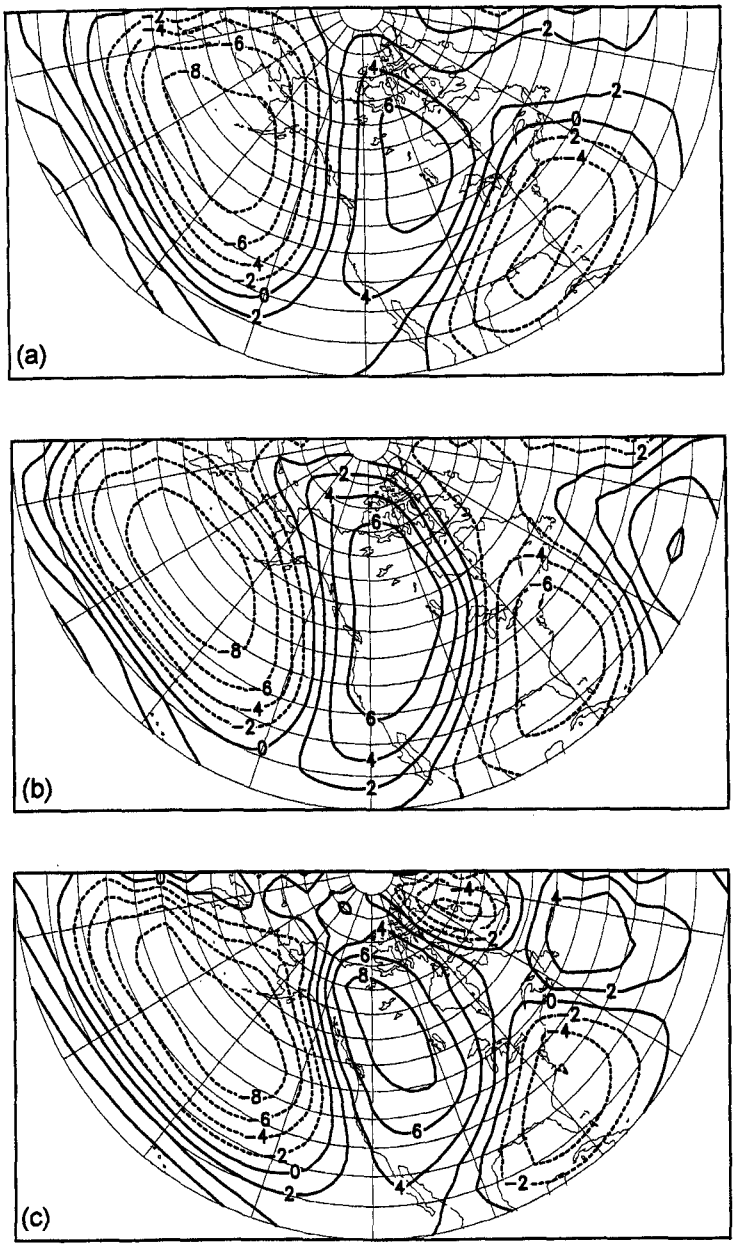

Figure 10. Homogeneous correlation patterns of 500 hPa height for EOF-1: (a) from GCM D 16×9 (deviations from the ensemble means for 16 winters); (b) from GCM Cli-SST (39 winters taken from GCM climatological SST integration); (c) from OBS 29 (re-analyses for 29 non-ENSO winters). The correlation has been multiplied by 10, with a contour interval corresponding to 0.2. See text for details.

correlation function associated with SVD-1 for the GCM 16 dataset (Fig. 4(b)) represents the SST-forced pattern, while the homogeneous correlation function associated with EOF-1 for the GCM D 16×9 dataset (Fig. 10(a)) is representative of the internal variability pattern. They are reproduced in Fig. 11(a) and (b) (with a different contour interval, and not multiplied by 10). The difference between these two patterns can be

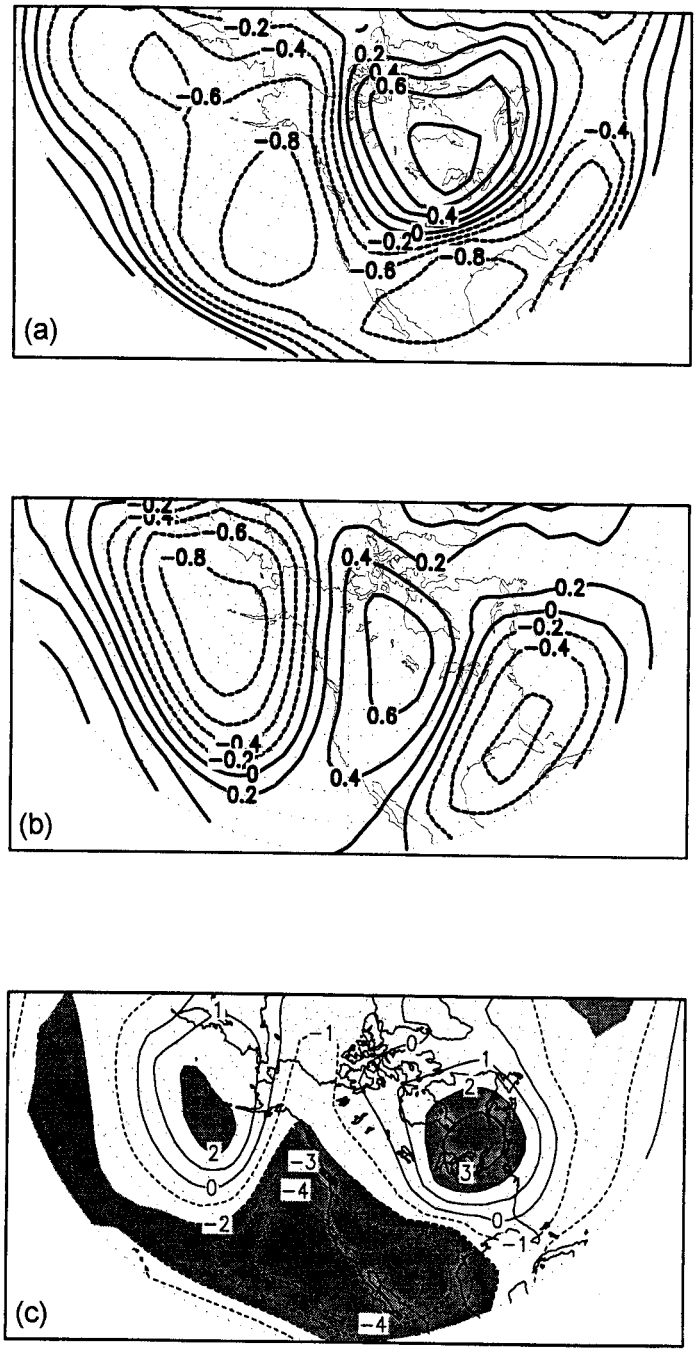

Figure 11. (a) Heterogeneous correlation pattern associated with SVD-1 for the GCM 16 (ensemble-mean dataset). (b) Homogeneous correlation pattern associated with EOF-1 for the GCM D 16×9 (deviations about ensemble mean). (c) Difference (a) minus (b). Shading indicates statistical significance at the 95% confidence level. The contour intervals are 0.2 in (a) and (b). See text for further details.

assessed by considering the difference between the correlations at each grid point separately. Using the Fisher transform, which yields an (approximately) normally distributed statistic (Thiébaux 1994), it is straightforward to test the statistical significance of the difference between two correlation values. The resulting statistic is shown in Fig. 11(c), where the 95% confidence level is indicated by shading. The differences between the patterns are seen to be significant over two broad areas. One extends westward from western continental North America over the Pacific Ocean to about 120°W, while the other (smaller) region is centred north-east of the Great Lakes. If the calculation is repeated using the external correlation map of Fig. 4(c) in place of the heterogeneous correlation map, the results are nearly identical. If, on the other hand, the heterogeneous correlation map is compared to the homogeneous correlation map associated with EOF-1 of the GCM Cli-SST dataset (Fig. 10(b)), the significant areas are expanded, covering most of the continental USA (not shown).

7. SUMMARY

In this paper we use the full GCM ensemble to separate clearly the dominant regional pattern of internal variability due only to sensitivity to initial conditions from the SST-forced response. The COLA GCM has demonstrated the realism necessary to be considered a reliable tool in making this distinction. Once the North Atlantic/Arctic-related variability in the observations and the GCM have been accounted for, the remaining GCM variability of seasonal means in the PacNA region (variance of GCM 16×9) compares very well with the remaining observed variability. The ratio of SST-forced variance to the GCM internal variance (GCM D16×9 or GCM Cli-SST) is statistically significant, particularly in the eastern Pacific, over Mexico, and over north-eastern North America.

Examination of this variability with regional EOF/SVD techniques leads to the identification of a very robust pattern, associated with the response to ENSO-related diabatic heating during the 16-year period. This pattern is seen in both the ensemble-mean record of GCM integrations (in which non-SST related variability has been approximately averaged out) and in the single record from observations. It arises as the leading (and dominant) EOF pattern, the leading (and dominant) mode in SVD analysis of the regional height field with tropical Pacific diabatic heating, and from regression of the height field on a time series (OBS 39) derived from NCEP re-analysis tropical heating for a long (39-year) record. Furthermore, this ENSO pattern is the same as that which arises from consideration of 10 strong ENSO winters obtained from observations solely on the basis of tropical Pacific SST data. It also agrees well with previous studies (e.g. Horel and Wallace 1981).

This pattern explains about 50% to 60% of the regional variance for both (ensemble-averaged) GCM and observations, and between 80% and 90% of the squared covariance with tropical diabatic heating. Because the observations include internal as well as SST-forced variability, the total observed regional variability is somewhat greater than in the simulated ensemble mean; hence the actual area-averaged explained variance for the ensemble-averaged GCM is only about 60% that of the observations. The area-averaged covariance of height with diabatic heating (see Table 1) in the GCM, in contrast, is 35% larger than in the observations, indicating a stronger degree of coupling between heating and response in the model.

The projection coefficients of all GCM seasonal means on the leading SVD mode of GCM ensemble means tend to cluster about their ensemble means. The ratio of the

variance of the ensemble-mean coefficients to the scatter of the projection coefficients about the ensemble mean is significant.

Deviations of GCM seasonal means about the ensemble mean are used to identify internal variability due only to sensitivity to initial conditions. Again, the hemispheric North Atlantic/Arctic hemispheric modes are excluded. The homogeneous correlation functions of the leading EOF (significantly distinct from the other EOFs) are calculated for: (i) the deviations of the nine GCM ensemble members about the ensemble mean for 16 winters (GCM D16×9); (ii) the 39 winters of the climatological SST GCM integration (GCM Cli-SST); and (iii) the 29 non-ENSO winters from observations. There is consistent agreement among all three datasets: the dominant pattern is closely related to the classical PNA pattern of WG. While there has been a suggestion (see Z) that this pattern is associated with *extratropical* North Pacific SST anomalies in the observations, the notion that the extratropical SST anomalies do not cause (but are rather a response to) atmospheric variations is consistent with the occurrence of the PNA in the GCM-D16×9 and GCM-Cli-SST datasets.

The SST-forced pattern is significantly different from the internal variability pattern over western North America and the adjoining eastern Pacific Ocean, and also over a region just north-east of the Great Lakes. This map of significance is computed by (for example) comparing the heterogeneous correlation pattern associated with the leading SVD of GCM ensemble means with the homogeneous correlation pattern of the leading EOF of GCM ensemble deviations, but the resulting map is robust to other appropriate choices for the correlation patterns.

8. Discussion

The distinction between ENSO-forced and internal variability presented here finds support from the observational results of Livezey and Mo (1987). They found that the simultaneous correlations of winter tropical SST with their PNA pattern (see Barnston and Livezey 1987) are not as high as the corresponding correlations with their tropical/northern hemisphere pattern, which strongly resembles our ENSO pattern of Figs. 4 and 8.

The methods of analysis used in this study to relate tropical Pacific diabatic heating with mid-latitude dynamics capture only the linear part of the relationship. Some evidence of the real asymmetries between the response to warm and cold events (Hoerling *et al.* 1997) is seen in the disparity between the amplitudes of these events in the EOF and SVD time series of Fig. 6. Since the methodology tries to fit one pattern for both cold and warm responses, it does not distinguish between them adequately. The present approach was necessitated by the modest number of calendar winters (16) for which ensemble GCM integrations have been made—only two cold events and three warm events are included. Future plans for carrying out ensemble integrations for a much larger number of calendar winters will enable better resolution of the asymmetries between warm and cold events.

While the structure of the diabatic heating fields in the dominant ensemble-mean SVD correlation patterns presented here (as well as the corresponding SST structure explored in S) makes it clear that this mode is related to ENSO forcing, the simulations were carried out with globally realistic SST boundary conditions. The role of non-ENSO SST, and in particular North Pacific SST-forcing on the height variations over the PacNA region is not resolved. Many studies have addressed this question, and it is not even clear that specifying SSTs in the North Pacific improves model simulations (see for example

Ferranti *et al.* 1994; Graham *et al.* 1994; Zhang *et al.* 1996). Resolution of this issue awaits the future.

9. Conclusions

The results presented here call into question a set of fairly fundamental tenets previously held. One is that the temporal variability of the mid-latitude atmosphere is not noticeably enhanced in the presence of SST fluctuations (Lau 1985, 1997); this assertion is contradicted by the current simulations using the COLA GCM, in which the presence of varying SSTs makes a large difference regionally in the mid-latitude variance of seasonal means. Another is the belief that the ENSO mid-latitude response pattern is dominated by an internal mode of the atmosphere (the PNA pattern), which would exist even in the absence of external (SST) forcing. We have demonstrated unambiguously in the context of the COLA GCM that the response forced by global SSTs, and strongly linked to ENSO-related diabatic heating, is quite distinct in the PacNA region from the internal variability pattern that dominates regionally. The applicability of these GCM results to the real atmosphere is supported by the fact that the COLA GCM has a realistic response to ENSO *both* in terms of the strength and the pattern of the anomalies, and also possesses realistic variability on the seasonal-mean time-scale. These findings are also strongly supported by consideration of the observed winters not considered to be strong ENSO events.

Acknowledgements

We would like to acknowledge many stimulating and helpful discussions with Professor J. M. Wallace and Dr Ben Kirtman, and the advice of the anonymous reviewers. This work was supported by the National Science Foundation (under grant ATM 93-21354), by the National Oceanic and Atmospheric Administration (under grant NA76GP0258) and by the National Aeronautics and Space Administration (under grant NAG5-4977).

Appendix

The North Atlantic/Arctic oscillation

(i) *The North Atlantic/Arctic pattern.* A hemispheric EOF analysis of the seasonal mean 500 hPa height for the northern hemisphere (20–80°N) was carried out for the following datasets: (a) GCM 16×9, (b) GCM Cli-SST, (c) OBS 39, and (d) GCM 16 (see section 2(e) for definitions). Table A.1 shows the percentage variance explained for the first three modes, and the associated uncertainty (according to North *et al.* 1982). In the GCM Cli-SST datasets the separation between the first and second modes is large compared to the uncertainty; for the other datasets the separation is less significant.

The homogeneous correlation patterns (multiplied by 10) associated with the first mode for each dataset are shown in Fig. A.1, plotted so that each contour corresponds to a correlation of 0.20. The leading EOF of the datasets GCM 16×9 (all seasonal means) and GCM Cli-SST, shown in Figs. A.1(a) and (b), is dominated by a large Arctic centre, with less intense features over North America, the North Atlantic, Asia and the Pacific. The patterns indicate a significant zonal-mean 'see-saw' between high and mid latitudes. They resemble the first EOF of the OBS 39 dataset (Fig. A.1(c)) which, however, has a stronger emphasis on the Atlantic region. For convenience we refer collectively to the patterns seen in Figs. A.1(a)–(c) as the North Atlantic/Arctic (NAA) pattern. The GCM

TABLE A.1. PERCENTAGE OF VARIANCE EXPLAINED BY EACH OF THE FIRST THREE HEMISPHERIC EOFs OF 500 hPa

Mode	GCM 16	GCM 16×9	GCM Cli-SST	OBS 39
1	35 (12)	23 (2)	38 (9)	27 (6)
2	24 (8)	21 (2)	15 (3)	19 (4)
3	16 (6)	9 (1)	10 (2)	9 (2)

The numbers in parentheses indicate the uncertainty according to North *et al.* 1982.

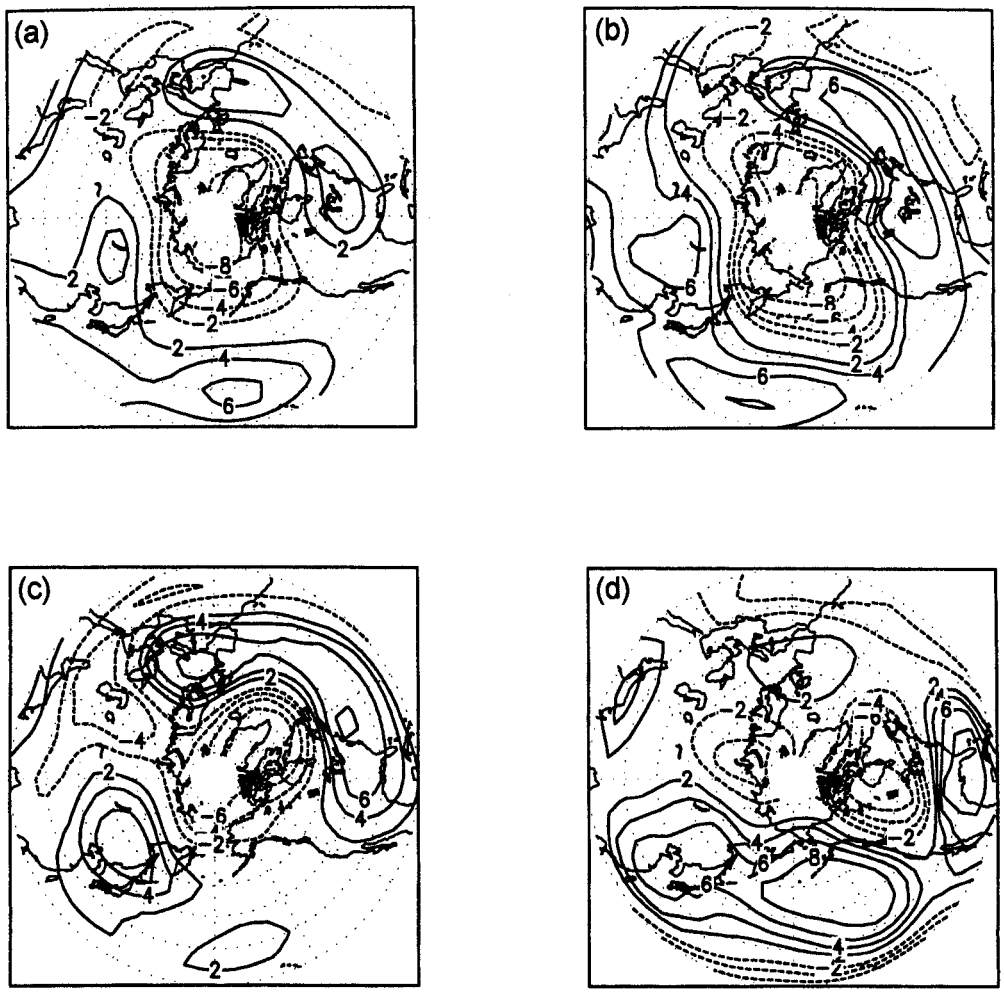

Figure A.1. Homogeneous correlation functions associated with EOF-1 for seasonal-mean hemispheric 500 hPa heights (20–90°N), with percentages of explained variance in parentheses: (a) from GCM 16×9 (all GCM integrations); (b) from GCM Cli-SST (39 winters of GCM climatological SST integration); (c) from OBS-39 winters (39 winters from re-analyses); (d) from GCM 16 (GCM ensemble means). All correlations have been multiplied by 10. The contour interval is 2, with the zero contour omitted. See text for further details.

16 pattern (Fig. A.1(d)), however, is basically a hemispheric version of the SST-forced pattern described in the paper, with a westward extension over the Pacific. Since in the GCM, the NAA pattern does not appear as the leading EOF when the ensemble-mean dataset is used, it is fair to conclude that this pattern is not related to the dominant ENSO SST variations over the 16-winter record. However, a relationship between the NAA pattern and mid-latitude SST variations is neither precluded in the GCM nor in the observations (Rodwell *et al.* 1999).

Removal of this mode from all the OBS datasets considered in this paper, is achieved by subtracting the EOF spatial pattern scaled by the coefficient (principle component) for all years, leading to a 39-winter filtered dataset. All subsequent analysis on any OBS dataset started from this filtered data. Similarly, all GCM integrations had the NAA pattern filtered out, by removal of the leading EOF of the GCM 16×9 dataset, and all GCM analyses used the filtered dataset.

(ii) *Definitions of SST-forced and total variance.* Following Rowell *et al.* (1995) and Scheffé (1959, p. 225), the SST-forced variance V_{SST} is related to the ensemble-mean variance V_{EM} and internal variance V_e as follows:

$$V_{EM} = V_{SST} + \frac{1}{n} V_e$$

where V_{EM} is the variance of the 16-winter ensemble means calculated in the standard manner, V_e is the variance of the ensemble members about the ensemble mean, averaged over all winters. V_{SST} is deduced from the above equation. The 'total' variance, V_{TOT}, is not given by the sum of V_{EM} and V_e, but is instead:

$$V_{TOT} = V_{SST} + V_e.$$

Figure 1(b) shows V_{TOT}, Fig. 2(a) shows V_e, and V_{SST} is used in Fig. 3.

REFERENCES

Barnston, A. G. and Livezey, R. E. 1987 Classification, seasonality and persistence of low-frequency atmospheric circulation patterns. *Mon. Weather Rev.*, **115,** 1083–1126

Bjerknes, J. 1966 A possible response of the atmospheric Hadley circulation to equatorial anomalies of mean temperature. *Tellus*, **18,** 820–829

1969 Atmospheric teleconnections from the equatorial Pacific. *Mon. Weather Rev.*, **97,** 163–172

Bretherton, C. S., Smith, C. and Wallace, J. M. 1992 An intercomparison of methods for finding coupled patterns in climate data. *J. Climate*, **5,** 541–560

Chen, W. Y. and Van Den Dool, H. M. 1997 Asymmetric impact of tropical SST anomalies on atmospheric internal variability over the North Pacific. *J. Atmos. Sci.*, **54,** 725–740

Deser, C. and Wallace, J. M. 1990 Large-scale atmospheric circulation features of warm and cold episodes in the tropical Pacific. *J. Climate*, **3,** 1254–1281

DeWitt, D. G. 1996 'The effect of the cumulus convection scheme on the climate of the COLA general circulation model'. COLA Tech. Memo. 27. (Available from the Center for Ocean–Land–Atmosphere Studies, 4041 Powder Mill Rd., Suite 302, Calverton MD 20705, USA

DeWitt, D. G. and Schneider, E. K. 1999 On the processes determining the annual cycle of equatorial sea surface temperature: A coupled general circulation model perspective. *Mon. Weather Rev.*, **127,** 381–395

Ferranti, L., Molteni, F. and Palmer, T. N. 1994 Impact of localized tropical and extratropical SST anomalies in ensembles of seasonal GCM integrations. *Q. J. R. Meteorol. Soc.*, **120,** 1613–1645

Graham, N. E., Barnett, T. P., Wilde, R., Ponater, M. and Schubert, S. 1994 On the roles of tropical and midlatitude SSTs in forcing interannual to interdecadal variability in the winter northern hemisphere circulation. *J. Climate*, **7,** 1416–1441

Hoerling, M. P., Kumar, A. and Zhong, M. 1997 El Niño, La Niña, and the nonlinearity of their teleconnections. *J. Climate*, **10,** 1769–1786

Horel, J. D. and Wallace, J. M. 1981 Planetary-scale phenomena associated with the Southern Oscillation. *Mon. Weather Rev.*, **109,** 813–829

Hoskins, B. J. and Karoly, D. J. 1981 The steady linear response of a spherical atmosphere to thermal and orographic forcing. *J. Atmos. Sci.*, **38,** 1179–1196

Kalnay, E., Kanamitsu, M., Kistler, R., Collins, W., Deaven, D., Gandin, L., Iredell, M., Saha, S., White, G., Woolen, J., Zhu, Y., Chelliah, M., Ebisuzaki, W., Higgins, W., Janowiak, J., Mo, K. C., Ropelewski, C., Wang, J., Leetma, A., Reynolds, R., Jenne, R. and Joseph, D. 1996 The NCEP/NCAR 40-year reanalysis projecct. *Bull. Am. Meteorol. Soc.*, **77,** 437–472

Kumar, A., Hoerling, M., Ji, M., Leetmaa, A. and Sardeshmukh, P. 1996 Assessing a GCM's suitability for making seasonal prediction. *J. Climate*, **9,** 115–129

Lau, N.-C. 1985 Modeling the seasonal dependence of the atmospheric response to observed El Niños in 1962–76. *Mon. Weather Rev.*, **113,** 1970–1996

1997 Interactions between global SST anomalies and the midlatitude atmospheric circulation. *Bull. Am. Meteorol. Soc.*, **78,** 21–33

Lau, N.-C. and Nath, M. J. 1994 A modeling study of the relative roles of tropical and extratropical SST anomalies in the variability of the global atmosphere–ocean system. *J. Climate*, **7,** 1184–1207

Livezey, R. E. and Mo, K. C. 1987 Tropical–extratropical teleconnections during the northern hemisphere winter. Part II: Relationships between monthly mean northern hemisphere circulation patterns and proxies for tropical convection. *Mon. Weather Rev.*, **115,** 3115–3132

Lorenz, E. N. 1956 'Empirical orthogonal functions and statistical weather prediction'. Science Report No 1, Statistical Forecasting Project, Department of Meteorology, Massachusetts Institute of Technology, USA

Molteni, F., Sutera, A. and Tronci, N. 1988 The EOFs of the geopotential eddies at 500 mb in winter and their probability density distributions. *J. Atmos. Sci.*, **45,** 3063–3080

North, G. R., Bell, T. L., Cahalan, R. F. and Moeng, F. M. 1982 Sampling errors in the estimation of empirical orthogonal functions. *Mon. Weather Rev.*, **110,** 699–706

Parker, D. E., Folland, C. K., Bevan, A. C., Ward, M. N., Jackson, M. and Maskell, K. 1995 Marine surface data for analysis of climate fluctuations on interannual to century timescales. Pp. 222–228 in *Natural variability on decade-to-century timescales*. Eds. D. G. Martinson, *et al.*, National Academic Press, Washington DC, USA

Renshaw, A. C., Rowell, D. P. and Folland, C. K. 1998 Wintertime low-frequency weather variability in the North Pacific–American sector 1949–93. *J. Climate*, **11,** 1073–1093

Reynolds, R. W. 1988 A real-time global sea surface temperature analysis. *J. Climate*, **1,** 75–86

Reynolds, R. W. and Smith, T. M. 1994 Improved global sea surface temperature analyses using optimum interpolation. *J. Climate*, **7,** 929–948

Rodwell, M., Rowell, D. P. and Folland, C. K. 1999 Oceanic forcing of the wintertime North Atlantic oscillation and European climate. *Nature*, **398,** 320–323

Rowell, D. P. 1998 Assessing potential seasonal predictability with an ensemble of multidecadal GCM simulations. *J. Climate*, **11,** 109–120

Rowell, D. P., Folland, C. K., Maskell, K. and Ward, M. N. 1995 Variability of summer rainfall over tropical North Africa (1906–92); Observations and modelling. *Q. J. R. Meteorol. Soc.*, **121,** 669–704

Saravanan, R. 1998 Atmospheric low-frequency variability and its relationship to midlatitude SST variability: Studies using the NCAR climate system model. *J. Climate*, **11,** 1386–1404

Sardeshmukh, P. D. and Hoskins, B. J. 1988 The generation of global rotational flow by steady idealized tropical divergence. *J. Atmos. Sci.*, **45,** 1228–1268

Scheffé, H. 1959 *The analysis of variance*. John Wiley & Sons Inc., New York, USA

Shukla, J. 1984 Predictability of time averages: Part II. Pp. 155–206 in *The influence of the boundary forcing, problems and prospects in long and medium range weather forecasting*. Eds. D. M. Burridge and E. Källën. Springer-Verlag, New York, USA

1985 Predictability. Pp. 87–122 in *Advances in Geophysics*. Vol. 28B, Academic Press, New York, USA

Shukla, J., Paolino, D. A., Straus, D. M., De Witt, D., Fennessy, M., Kinter, J. L., Marx, L. and Mo, R. 2000 Dynamical seasonal prediction with the COLA atmospheric model. *Q. J. R. Meteorol. Soc.*, **126,** 2265–2291

Simmons, A. J. 1982 The forcing of stationary wave motion by tropical diabatic heating. *Q. J. R. Meteorol. Soc.*, **108,** 503–514

Simmons, A. J., Wallace, J. M. and Branstator, G. W. 1983 Barotropic wave propagation and instability, and atmospheric teleconnection patterns. *J. Atmos. Sci.*, **40,** 1363–1392

Straus, D. M. and Shukla, J. 1997 Variations of midlatitude transient dynamics associated with ENSO. *J. Atmos. Sci.*, **54,** 777–790

Thiébaux, H. 1994 *Statistical data analysis for ocean and atmospheric sciences*. Academic Press, New York, USA

Thompson, D. W. J. and Wallace, J. M. 2000 Annular modes in the extratropical circulation. Part I: Month-to-month variability. *J. Climate*, **13,** 1000–1016

Trenberth, K. E. and Hurrell, J. W. 1994 Decadal atmosphere–ocean variations in the Pacific. *Clim. Dyn.*, **9,** 303–319

Wallace, J. M. and Gutzler, D. S. 1981 Teleconnections in the geopotential height field during the northern hemisphere winter. *Mon. Weather Rev.*, **109,** 784–812

Wallace, J. M., Zhang, Y. and Lau, K.-H. 1993 Structure and seasonality of interannual and interdecadal variability of the geopotential height and temperature fields in the northern hemisphere troposphere. *J. Climate*, **6,** 2063–2082

Yulaeva, E. and Wallace, J. M. 1994 The signature of ENSO in global temperature and precipitation fields derived from the microwave sounding unit. *J. Climate*, **7,** 1719–1736

Zhang, Yuan, Wallace, J. M. and Iwasaka, N. 1996 Is climate variability over the North Pacific a linear response to ENSO? *J. Climate*, **9,** 1468–1478